

## Supplementary information

# Oxygen-free discontinuous dewetting in a degassed mold for anisotropic colloidal hydrogel microparticle synthesis

Jiwoo Kim,<sup>a</sup> Jun Hee Choi,<sup>a</sup> Jeongmin Kim,<sup>b</sup> Jihyun Kim,<sup>b</sup> Yoon Ho Roh,<sup>\*cd</sup> and Ki Wan Bong<sup>\*a</sup>

<sup>a</sup> Department of Chemical and Biological Engineering, Korea University, Seoul, 02841, Republic of Korea

<sup>b</sup> Department of Chemical and Biological Engineering, Seoul National University, Seoul, 08826, Republic of Korea

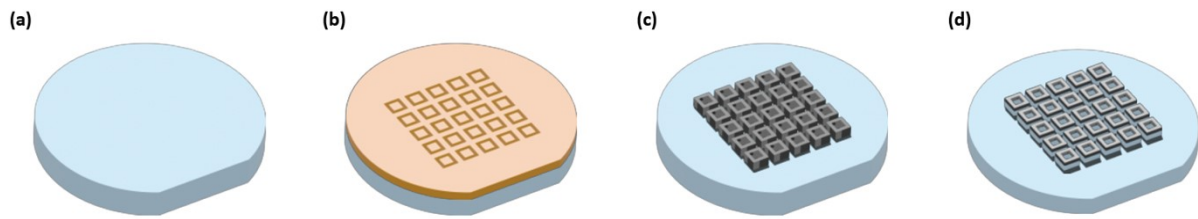
<sup>c</sup> Department of Energy and Chemical Engineering, Incheon National University, Incheon, 22012, Republic of Korea

<sup>d</sup> Innovation Center for Chemical Engineering, Incheon National University, Incheon 22012, Republic of Korea

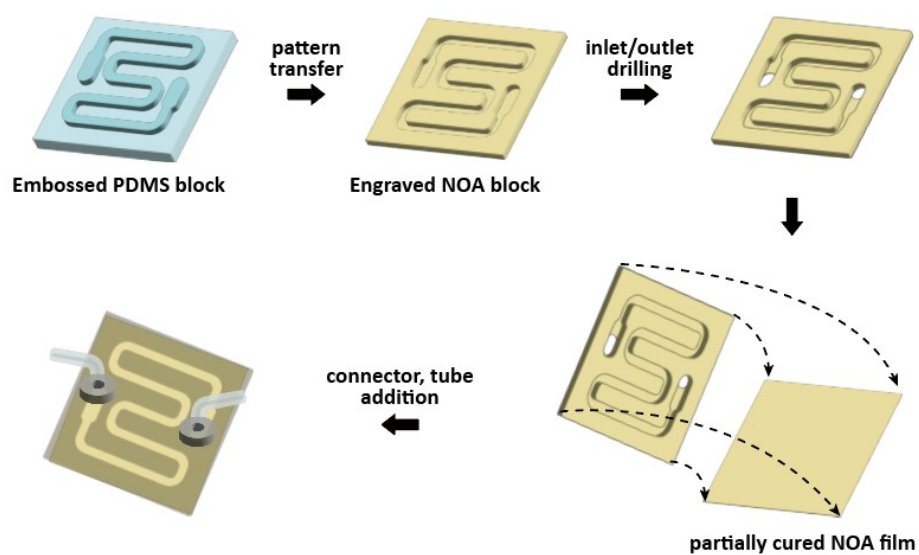
\*Correspondence: [bong98@korea.ac.kr](mailto:bong98@korea.ac.kr)

## Table of Contents

- Figure S1.** Schematics of silicon wafer patterning process.
- Figure S2.** Fabrication process of imaging flow cytometry device.
- Figure S3.** Deep learning-based hydrogel microparticle analysis program.
- Figure S4.** Atomic force microscopy of the silicon wafer.
- Figure S5.** Scanning electron microscopic images of the silicon wafer.
- Figure S6.** Fluorescent images of the particles used in Brownian motion tracking.
- Figure S7.** The synthesis of a few hundred micrometer-scale hydrogel particles.
- Figure S8.** The clear visualization of the imaging flow cytometry results of 10  $\mu\text{m}$  particles in Figure 4b.
- Figure S9.** SEM images of cylinder particles with 775 nm of radius and 600 nm of height.
- Figure S10.** Anisotropic colloidal particles made of NOA epoxy resin.

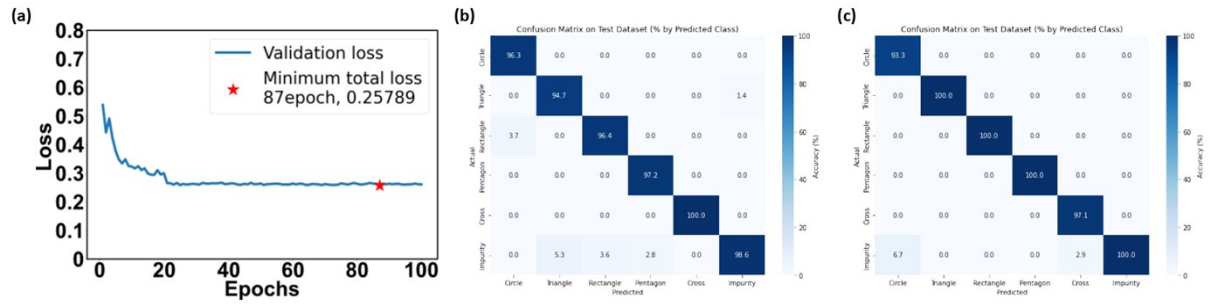


**Figure S1. Schematics of silicon wafer patterning process.** (a) Bare Si wafer. (b) A photoresist layer was spin-coated and patterned via conventional photolithography to define the micropattern array. (c) A Cr layer was deposited by electron-beam evaporation, followed by a lift-off process to form Cr etch mask. (d) The underlying Si was etched via reactive ion etching process with the Cr mask.



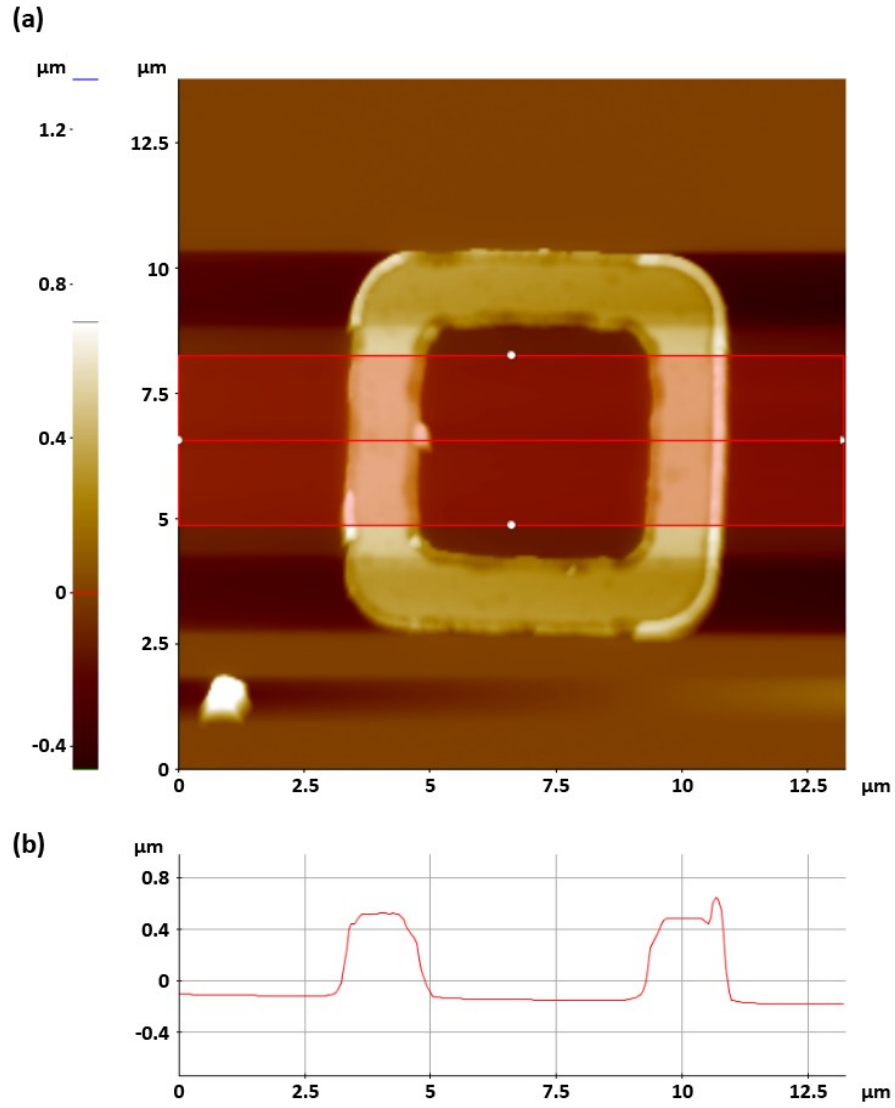
**Figure S2. Fabrication process of imaging flow cytometry device.**

Figure S2 illustrates the fabrication process of imaging flow cytometry (IFC) device. First, a PDMS block with embossed pattern of the channel was utilized to transfer the pattern to the NOA block with soft lithography. The channel pattern-engraved NOA block was drilled at the particle inlet and outlet area with a  $D = 1.5$  mm biopsy punch. After attaching the engraved NOA block to a partially cured NOA film,  $3 \text{ mW/cm}^2$  UV for 3 min was used for full curing of the stacked NOA block. Finally, the connector for connecting the Tygon tube was added to the inlet and outlet holes. The fabricated IFC devices were stored at a  $70^\circ\text{C}$  oven.



**Figure S3. Deep learning-based hydrogel microparticle analysis program.** (a) Validation loss curve over training epochs, with the minimum observed at epoch 87. (b) Confusion matrix showing the classification accuracy of the model for shape-encoded particles with a characteristic size of 50  $\mu\text{m}$ . (c) Confusion matrix for particles with a characteristic size of 10  $\mu\text{m}$ .

We employed the widely used Mask R-CNN model, a representative instance segmentation deep learning architecture, to classify shape-encoded particles and identify their pixel-level locations. A total of 1,207 images were used for training, and the dataset was split into training and validation sets at an 8:2 ratio. All other training settings followed previous reports. Subsequent procedures, including particle classification, and fluorescence intensity measurement using the trained deep learning model, were also carried out following the methods described in prior studies.



**Figure S4. Atomic force microscopy of the silicon wafer.** (a) The AFM image of the silicon wafer. The color of each pixel indicates the height of the patterns. (b) The height profile of the silicon wafer from the image in (a). The height is obtained by averaging the height values along the x-axis within the red-boxed region.

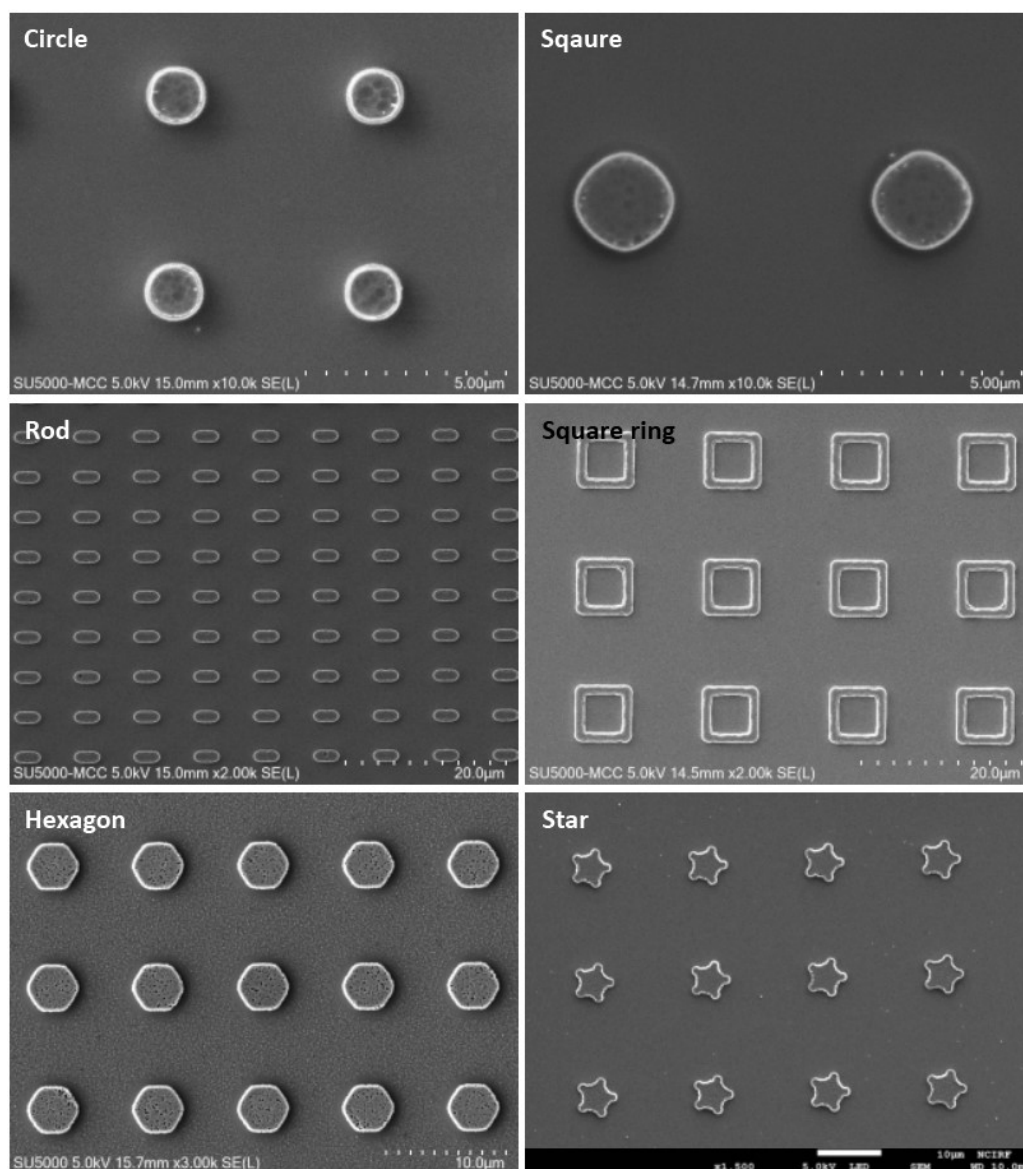
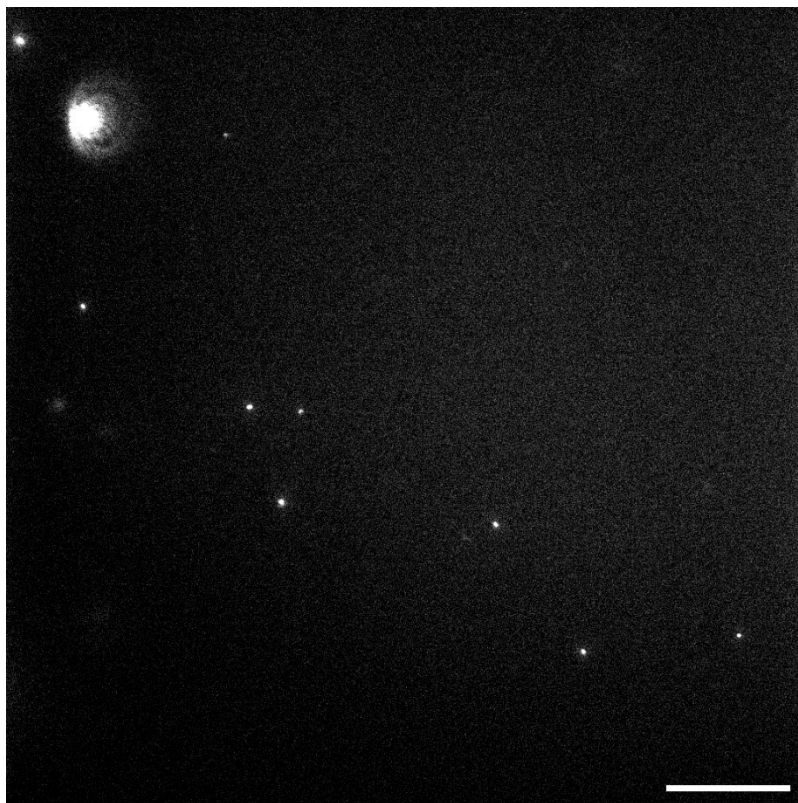


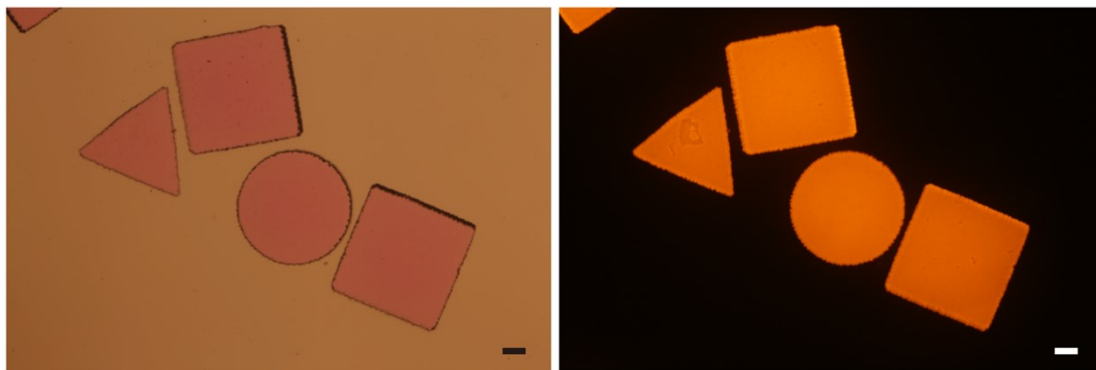
Figure S5. Scanning electron microscopic images of the silicon wafer with shapes of circle, square, rod, square ring, hexagon and star. The size of the scale bars are included at the right bottom of each image.



**Figure S6. Fluorescence image of the particles used in Brownian motion analysis. The scale bar is 50  $\mu\text{m}$ .**

The fluorescence image of the colloidal hydrogel particles for particle tracking. The particles were tracked from the moment they enter the focal plane to the moment they leave with 50 ms of time interval. The trajectory of each particles was used for Brownian motion analysis.





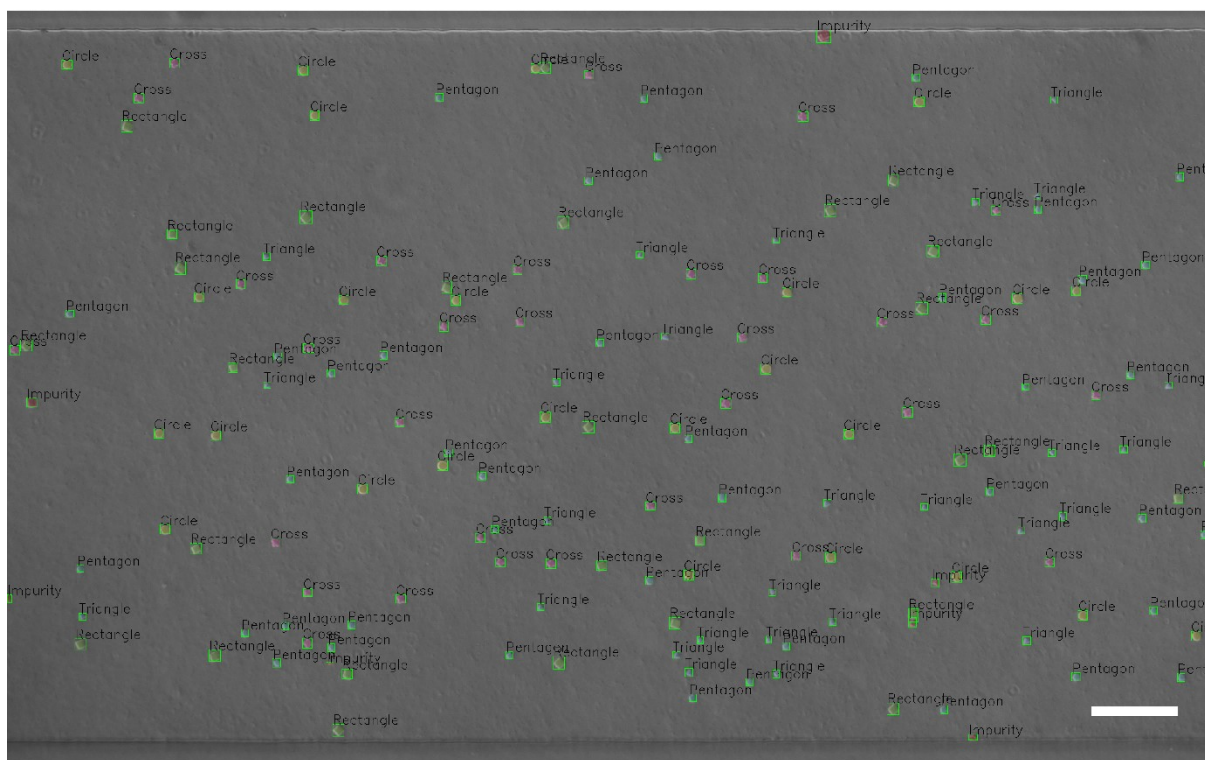
**Figure S7. The bright field (left) and fluorescence (right) images of a few hundred micrometer-scale hydrogel particles with shapes of circle, triangle and square. The scale bars are 100  $\mu\text{m}$ .**

Figure S7 displays the images of a few hundred micrometer-scale hydrogel particles synthesized with oxygen-free discontinuous dewetting in a degassed mold. The length of each side of the triangle and square particles is 500  $\mu\text{m}$ . The diameter of the circle particles is 500  $\mu\text{m}$ . The particles were labelled with rhodamine-B by adding rhodamine-B-acrylate to the precursor. The particles had uniform shapes, highly matching the master mold, and uniform fluorescence intensities.

The size limitation of oxygen-free discontinuous dewetting in a degassed mold platform is mainly determined by the inherent resolution of the mold material, PDMS. In our current setup, we used PDMS as the mold material for its transparency, cost-effectiveness, and broad usage among various fields. Most importantly, the porous structure of the PDMS is well-suited to act as a negative pressure generator for precursor liquid filling when treated with vacuum. Due to the elasticity and feature fidelity of PDMS, the smallest mold features that can be stably replicated without deformation are typically around 500 nm.<sup>1</sup> Below this threshold, surface tension and mold relaxation during peeling-off process result in rounding and collapse of fine features, preventing the formation of well-defined particles. In fact, the patterns in the master mold of sizes smaller than 600 nm did not transfer with good fidelity to the PDMS mold. Therefore, we concluded that the smallest synthesizable feature size is 600 nm.

On the other hand, the upper size limit is dictated by the filling dynamics of the precursor liquid into the mold cavity. As the feature size increases, capillary filling becomes slower and air entrapment within the cavity becomes more likely, which may lead to incomplete filling or nonuniform polymerization. We verified that particles with dimensions up to 500  $\mu\text{m}$  can be reliably fabricated without deformation or filling defects (Figure S7).

To summarize, the effective size range of our platform spans from 600 nm to 500  $\mu\text{m}$ , covering both colloidal and microscale regimes.



**Figure S8.** The clear visualization of the imaging flow cytometry results of 10  $\mu\text{m}$  particles in Figure 4b. The scale bar is 50  $\mu\text{m}$ .

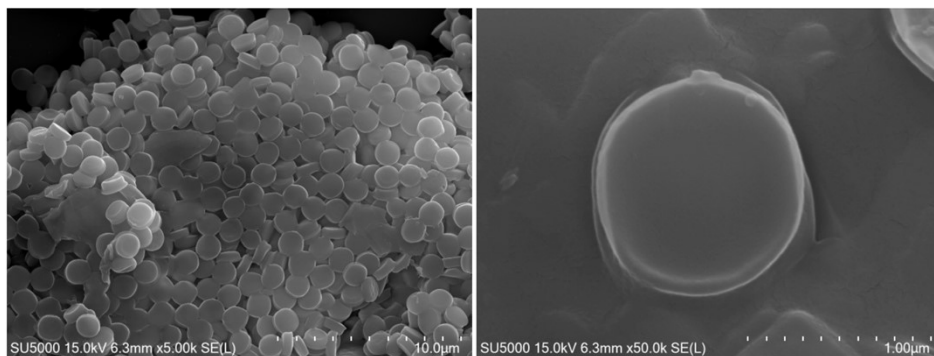


**Figure S9.** SEM images of cylinder particles with 775 nm of radius and 600 nm of height. The particles were made with NOA 81 instead of porous hydrogels to prevent shrinkage during drying process and retain the morphological features.

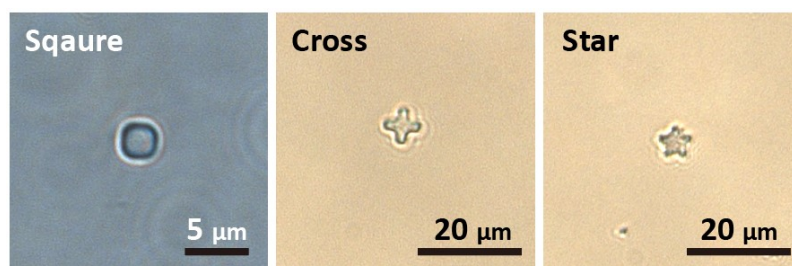


**Figure S10.** Anisotropic colloidal particles made of NOA epoxy resin. The particle shapes are square, cross and star. After discontinuous dewetting process in oxygen-free condition, 365 nm UV was irradiated for 1 min with intensity of 207 mW/cm<sup>2</sup>.

## References

1. C. Con and B. Cui, *Nanoscale Research Letters*, 2013, **8**, 394.